Dual-plasmonic Au/graphene/Au enhanced ultrafast, broadband, self-driven silicon Schotty photodetector

To cite this article before publication: Li Wang *et al* 2018 *Nanotechnology* in press https://doi.org/10.1088/1361-6528/aae360

Dual-plasmonic Au/graphene/Au enhanced ultrafast, broadband, self-driven silicon Schotty photodetector

Li Wang, Shu-Juan He, Kui-Yuan Wang, He-Hao Luo, Ji-Gang Hu,[a] Yong-Qiang Yu, Chao Xie, Chun-Yan Wu, Lin-Bao Luo[a]

School of Electronic Sciences and Applied Physics and Anhui Provincial Key Laboratory of Advanced Materials and Devices, Hefei University of Technology, Hefei, Anhui 230009, China

[a] Correspondence should be addressed to Email: jghu@hfut.edu.cn (J. G. Hu), E-mail: luolb@hfut.edu.cn (L. B. Luo)

Abstract

High-performance photodetectors are desirable for various applications, including multi-wavelength image sensing, communication and safety monitoring. In this study, we report the construction of dual-surface plasmon enhanced silicon Schotty photodetector using Au nanoparticles (NPs)/graphene/Au NPs hybrid structure as electrode. It was found that the as-assembled device exhibited broad sensitivity ranging from ultraviolet to near-infrared light (360-1330nm) at room temperature, with high response speed of 360 ns and 3dB bandwidth of 780 kHz at zero bias. Further theoretical simulation based on finite-element method (FEM) revealed that the good device performance is associated with the contribution of the Au NPs/graphene/Au NPs electrode: Intense dual plasmonic resonance couplings is induced in hybrid structure of two layers metallic NPs separated by uniform monolayer graphene. It not only can enhance light trapping and the localized electric field at the resonant and off-resonant wavelength region, but also are beneficial for the tunneling of hot electrons. This work demonstrated the great potential of the dual plasmonic resonance couplings in optoelectronic devices and will lead to the development of advanced plasmonic devices.

Keywords: graphene, localized surface plasmon resonance, photodetector, hot electrons, fast response speed.

Introduction

Photodetectors are the mainstay of imaging systems, environmental surveillance, communications and space exploration[1-6]. Present photodetection technologies rely primarily on photoactive semiconducting materials with certain band gaps corresponding to distinct spectral ranges. Silicon (Si) is prevalent in electronics and also a dominant material in photonics for its natural advantage in monolithic integration of optics and electronics [7]. However photonic components seems unlikely to be all Si-based. Si shows weak absorption beyond wavelength of 0.9μm and less than 0.4μm due to its bandgap (1.12eV), indirect absorption mechanism, low photo-responsivity caused by high reflection coefficient and shallow penetration depth of UV light in Si[7-9].

Plasmonics can induce dense electro-magnetic (EM) hot spots with high field enhancement over a large area[10], even in the off-resonant wavelength region[8][11]. It is worth noting that harvesting hot electrons from plasmonic nano-particles (NPs) can circumvent the challenge of detecting photons with energies below the bandgap of semiconductor[8][12-13].The attachment of plasmonic NPs to semiconductor surface has proved to be beneficial to increasing photocurrent, improving response speed and extending the response spectrum of photodetector[10][14]. The effective absorption cross-section of semiconductor material and the number of hot electrons both increases with the strength and density of EM hot spots[15-16]. It is well established that EM field is mainly determined by the inter-particle distance of NPs. Generally, intense dual plasmonic resonance couplings should be induced, if two layers of metallic NPs are separated by suitable ultrathin two-dimensional (2D) material uniformly. This will lead to remarkably elevated localized electric fields and stronger hot spots with high

density[17-18], which can be used to improve the performance of photoelectric device.

As a robust and stable 2D material, monolayer graphene has high carrier mobility and light transmittance[19-20]. It is an ideal material to be used as electrode material in optoelectronic devices[21-22] and also the intermediate material in the dual plasmonic resonance couplings hybrid structure[23-26]. So far the performance and detection wavelength region of Si can be improved and broadened by plasmonics, only when monolayer noble metal nanostructures combining with the texture of Si surface[8][27]. In this work, we propose a dual-plasmon enhanced planar Si Schotty photodetector with a Au NPs/graphene/Au NPs hybrid electrode. The device exhibited a broadband response ranging from UV to near-infrared light (360-1330nm), with a high response speed of 360ns and 3dB bandwidth of 780 kHz at zero bias. Further analysis based on theoretical simulation revealed that the high device performance mainly originates from the contribution of hybrid Au NPs/graphene/Au NPs electrode. This work demonstrated the great potential of the dual plasmonic resonance couplings in optoelectronic devices, and will lead to the development of advanced active plasmonic devices and high-bandwidth on-chip plasmonic circuits.

2. Experiment

2.1 *Device fabrication*

The dual-plasmon enhanced planar Si Schotty photodetector with a hybrid Au NPs/graphene/Au NPs electrode was fabricated on commercially available lightly-doped n-type Si wafer substrates (resistivity:~1-10Ωcm, thickness: 240±10μm) with a 300 nm SiO_2 layer. The main fabrication process is displayed in Figure 1a. Si substrate was cut into small pieces with an area of about 1×1 cm^2. Photolithography was then used to pattern windows

with the sizes of 0.2×1 cm^2. SiO_2 in the window was subsequently etched away by using a buffered oxide etchant, where Si was exposed for fabricating Schottky-junction with Au NPs/graphene/Au NPs hybrid electrode. To fabricate hybrid electrode, 5 nm Au films were first deposited on the substrate at a rate of about $1Ås^{-1}$ under a pressure of about 10^{-3} Pa by electron beam deposition, and turned into Au NPs by following rapid annealing in a protective atmosphere of argon at 500°C for 30min. Afterwards CVD-grown graphene was transferred onto the top of Si wafer covering the window[9]. The sample was then baked at 60°C for 5min to improve the adhesion with graphene. After that, another 5 nm Au film was deposited on the top of graphene film and annealed at 250 °C for 30 min to form the second layer of Au NPs. For comparison, other two kinds of Si Schottky photodetector were prepared, whose schematic structures are shown in Figure S1(a-b) in the Supporting Information. One is constructed by n-type Si wafer and 10 nm Au film, named D1. And the other is fabricated with n-type Si wafer and Au NPs/graphene electrode, named D2. Its Au NPs were also obtained by annealing Au films of 5 nm in a protective atmosphere of argon at 500°C for 30min.

2.2 *Characterization and measurement*

The morphology of Au NPs was examined by FESEM (Philips XL 30 FEG), and Raman study of the graphene film was performed on a Raman spectrometer (JY, LabRAM HR800). *I-V* curves of devices were measured on the semiconductor characterization system (Keithley 4200-SCS). To determine the spectral response and time response, lasers of different wavelengths and a xenon lamp equipped with a monochromator (Omni-l300) were used as the illumination source. The measurement of response speed were carried out using a

self-built setup composed of an oscilloscope (Tektronix, TDS2012B) and a pulsed light illumination, which was obtained by a mechanically rotating chopper (LEoc120) operated at different frequency. During testing, the fast-switching photovoltage was collected by the oscilloscope.

2.3 *Theoretical simulation*

The proposed structure is simulated by using a home-made program based on the finite-element method (FEM). The size of the structure is mainly obtained from SEM images. Surface wave is excited by a surface current from the top side to model the solar spectrum with wavelength range 200-1200nm. Both scattering boundary condition and perfectly matched layers have been used to absorb any reflected and transmitted fields. The boundary condition implies that our substrate and free-space are semi-infinite to keep the simulation as close to the real world as possible. The monolayer graphene is treated as an ultrathin film layer with a thickness of Δ=0.35nm. In addition, the device is simulated in the air whose permittivity is 1. And the permittivity of Si and Au is obtained from the Sopra SA Company database.

3. Results and discussion

Figure 1a shows the fabrication process of planar Si Schottky photodetector (D3) with Au NPs /graphene/Au NPs hybrid electrode. After depositing and annealing gold film on the monocrystalline Si wafer, a layer of Au NPs were obtained on Si substrate. Then graphene film was transferred onto the surface of Au NPs. After that, another layer of Au film was deposited and annealed on graphene to form Au NPs/graphene/Au NPs sandwich structure (Detail fabricated procedure can be seen in the Experimental Section.). Figure 1(b-c) shows

the schematic structure and photograph of D3, respectively. The size statistics of Au NPs in the first layer were obtained from the SEM image (Fig. 1d). It can be seen that the gold particles obtained by annealing at 500ºC, are mainly spherical with a diameter about 40nm. This indicated that the contact area of Si and Au shrank to be about 48% of the original value after turning Au film into NPs. And the diameter of the Au NPs in second layer is about 60nm (Fig. 1e) for its lower annealing temperature (250ºC). It can be seen clearly that Au NPs of the second layer and the first layer are interlaced and separated by a transparent graphene film. There are two major scattering peaks in the Raman spectrum of the graphene film: 2D-band peak at ~ 2682 cm^{-1} and G-band peak at ~ 1589 cm^{-1}(Figure 1f). The intensity ratio of I_{2D}:I_G is about 2, indicative of monolayer graphene[19][28-30]. Thereby the gap between the two layers of Au NPs should be uniform and about 0.35 nm due to the separation of graphene[31].There are three peaks, labeled as G, 2D and D, respectively, in the spectrum of AuNP/graphene/AuNP structure. The D peak due to defect is probably generated at the AuNP/graphene interface during annealing process[32]. Furthermore, compared with pure graphene, the intensity of G peak and 2D peak increased substantially after the functionalization with plasmonic Au NPs.

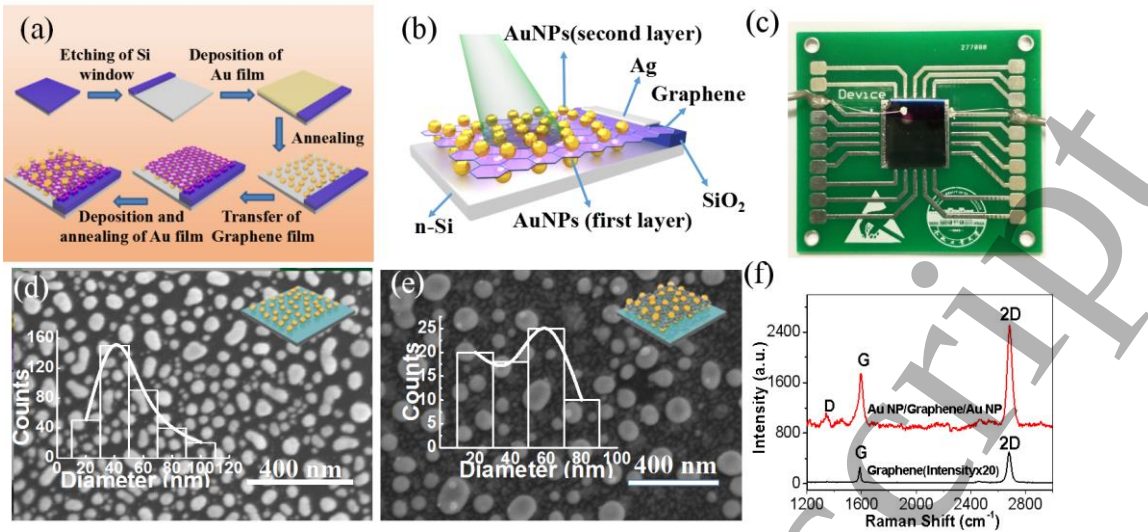

Figure 1(a) Illustration of the step-wise flow chart of fabricating dual-plasmon enhanced Si Schottky photodetector with Au NPs /graphene/Au NPs hybrid electrode. (b) The schematic view of the dual-plasmon enhanced photodetector. (c) A digital photograph of the device. (d-e) Typical SEM images of the first layer Au NPs and the second layer Au NPs in Au NPs/graphene/Au NPs hybrid electrode. The insets show the size histogram of the Au NPs and its corresponding Gaussian fits. (f) Raman spectrum of pure graphene and the Au NPs/graphene/Au NPs hybrid structure.

To investigate the effect of electrode structure on photodetector, *I-V* curves of D1, D2 and D3 were measured in darkness and under white light (Fig. 2a). D3 and two reference samples (D1 and D2) all show obviously rectification behavior for the Schottky junction existed between n-type Si and Au as well as n-type Si and graphene[9][33]. In addition, D3 and D2 exhibit obviously smaller dark current and larger turn-on voltage than D1. The Schottky barrier height of D1, D2 and D3 is calculated to be 0.89, 0.95 and 0.96eV, respectively, according to the formula:$\varphi_B=(KT/e)\ln(A^*T^2/J_s)$[34]. Here A* is Richardson constant for the n-lightly doped Si, and J_s is the current density. This indicates that annealing process can lead to the increase of Schottky barrier height for the improvement of junction quality. Under pulsed incident white light, D3 shows the largest photo-current and I_{on}/I_{off} ratio among the three photodetectors (Fig. 2b). And its I_{on}/I_{off} ratio increased with negative bias voltage approaching 0V (Fig. 2c). Figure 2d shows the logarithm plot of the I-V curve with absolute

value of the D3 current. There is obvious photocurrent existed when no external voltage was applied. The photoresponse of the device is stable and repeatable at 0V bias, even after 50 cycles of white light illumination (Fig. 2e).

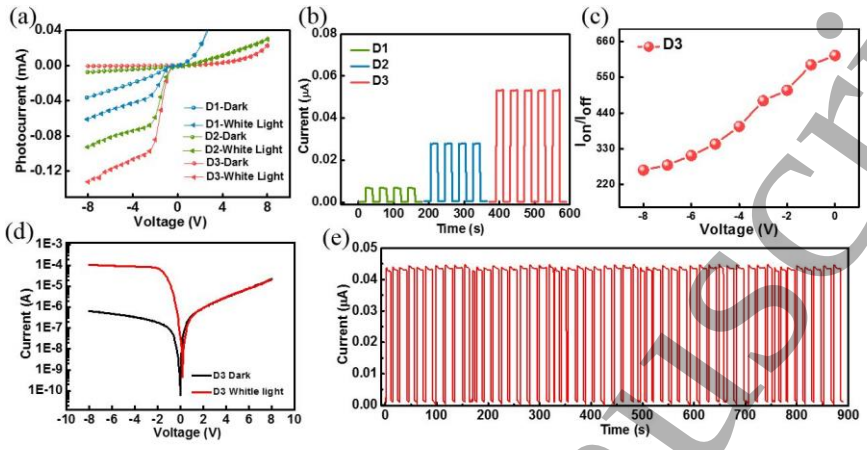

Figure 2 (a) Current-voltage *(I-V)* curves of device D1, D2 and D3 under darkness and white light. (b) Time responses of D1, D2 and D3 under white light illumination at bias voltage of -1V. (c) I_{on}/I_{off} ratio of D3 with the change of negative bias voltage. (d) Logarithm plot of the I-V curve with absolute values of D3 current under darkness and white light. (e) Stability test of D3 under 50 cycles of switch operation at 0V bias.

The performance of D3 and other two reference devices were compared under lights with four typical wavelengths of 365 nm (UV), 532 nm(Vis), 980 nm(NIR), and 1330nm (NIR) as excitation sources in different spectral range (Fig. 3(a-d)). It is shown that the performance of D2 is obviously enhanced, compared with D1, which is understandable considering the fact that transforming Au film to Au NPs can reduce reflectance and help trap the incident light for the plasmonic resonance couplings. What is more, the D3 exhibits more pronounced photosensitivity $S(=[(I_{ph}-I_{dark})/I_{dark}]\times 100\%)$[35] than D2 (Fig. 3(e-f)). Further analysis also reveals that the enhancement ratio of D3 to D2 is different on different wavelength (Fig. 3f). Under the irradiation of 532nm and 1330nm light source, the photoresponse of D3 is significantly better than D2.

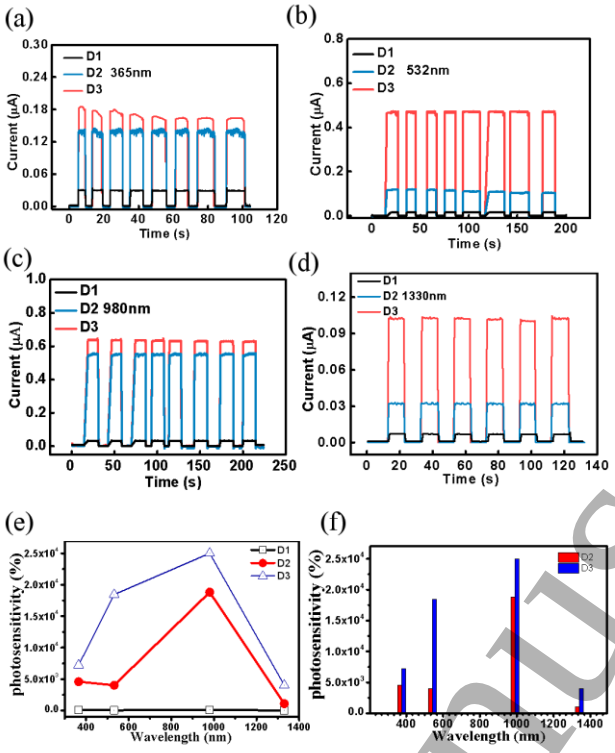

Figure 3 Time-resolved photoresponse of D1, D2 and D3 are shown in (a) 365nm (UV light) irradiation, (b) 532nm (Vis light) irradiation, (c) 980nm (NIR light) irradiation, and (d) 1330nm (NIR light) irradiation with intensity of 0.6mW/cm^2; the bias voltage was fixed at 0V. (e) Photosensitivities of D1, D2 and D3 under lights with four typical wavelengths of 365(UV), 532(Vis), 980 (NIR), and 1330nm (NIR).(f) Corresponding bar chart of the photosensitivities of D2 and D3.

The above finding is further confirmed by the responsivity of D1, D2 and D3 in the spectrum rage of 320-1330nm at 0V (Fig. 4a). Compared with D2, the responsivity of D3 is enhanced in the range of 1000-1300nm. Meanwhile there is an obvious enhancement at 530nm. This peak shows that there is strong plasma resonance of Au NPs[14], which should be caused by special AuNPs/graphene/Au NPs hybrid structure. The obvious responsivity in 1000-1330nm range is very abnormal for Si-based photodetctors which is usually unable to detect NIR region beyond 1200nm. The photoresponsivity of D3 is 24.17mA W^{-1} at 1330nm, which is comparable to reported plasmonic and non-plasmonic NIR detector of textured Si[8][36-37]. As expected, dual plasmonic resonance couplings extends the response of Si-based photodiodes into the NIR region, which is confirmed by the comparison of D3 to Si/monolayer graphene

photodetector too (Fig. S2).

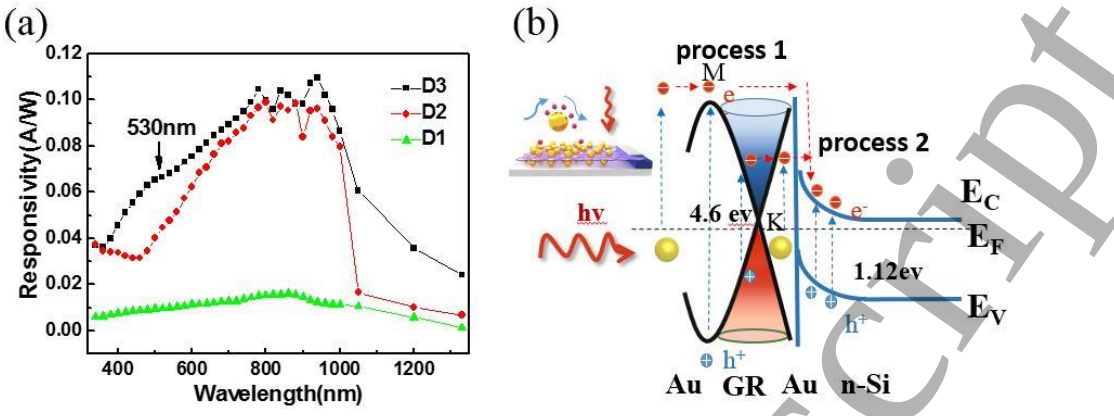

Figure 4 (a) Wavelength-dependent photoresponsivity of D1, D2, and D3 calculated at a fixed bias voltage of 0V with light intensity of about 0.35μW. (b) Energy band diagram of the Schottky junction.

There should be actually two kinds of process in D3 producing photocurrent (Fig. 4b). One is the separation of electron-hole pairs by the internal electric field after the photo-excitation in Si (process 2), the other is harvesting the hot electron from the Au NPs/graphene/Au NPs hybrid structure (process 1). As discussed above, the gap between the two layers of Au NPs is on the scale of sub-nanometer for the separation of monolayer graphene. Plasmonic particles with smaller gaps can lead to larger EM field enhancements[16][38-39]. As a consequence, the special Au NPs/graphene/Au NPs hybrid structure would produce stronger hot spots than solely Au NPs due to the dual plasmonic resonance couplings. This will lead to strong internal photoemission process in D3, since the number and energy of hot electrons grows with the strength of hot spots[16]. A large number of hot electrons with high energy multiply after part of the incident light is absorbed by Au NPs and graphene. And the small thickness of graphene can effectively shorten the distance of hot electron diffusing to the Schottky interface. All these ensure that a large number of hot electrons have enough energy to cross over the Schottky barrier, and contribute to the total photocurrent of the device. And this part

of photocurrent should be the main factor for improving the performance of Si photodetector D3 in the UV and IR region.

The experimental results have been confirmed by theoretical simulation. Figure 5a shows the FDTD simulation results for reflectance spectrum of Si film, Au film, single layer AuNPs and Au NPs/graphene/AuNPs. The reflectance is greatly weakened in the Au NPs/graphene/AuNPs hybrid structure. It should be attributed to multiple effects including the increased dimensions of Au NPs and the presence of graphene with enhanced light-matter interactions[40]. Figure 5b illustrates the electric field energy distribution of the Au NPs/graphene/AuNPs hybrid structure in the xz-plane. According to the size of Au NPs in the device D3, the diameters of NPs of the first and second layer are set to be 40 nm and 60 nm respectively. It can be clearly seen that localized electrical field is mainly distributed at the space between horizontal or vertical adjacent Au NPs and the space between Au NPs and Si. This indicates that dual plasmonic resonance couplings can effectively affect the light-matter interaction not only in Au NPs/graphene/Au NPs hybrid structure but also in Si. Notably, the electrical field is strongly enhanced in the gap between vertical Au NPs for the separation of graphene. Further numerical simulations show that electric field intensity will decrease when the diameter of Au NPs of the second layer increases from 60nm to 80nm, leading to an increase of reflectance (Fig. 5(c-d)). These reveal that the morphology of Au NPs influences the coupling effect greatly.

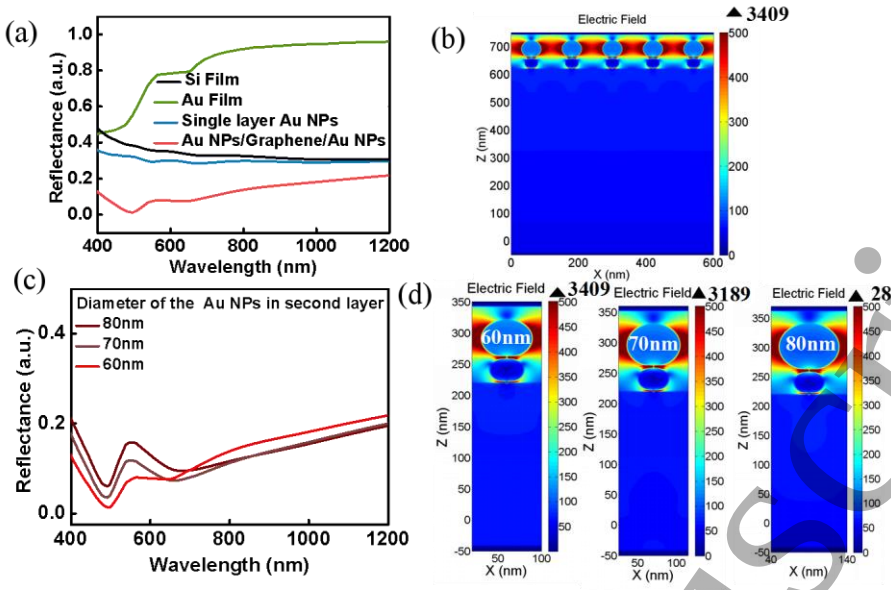

Figure 5 (a) Simulated reflectance spectrum of Si film, Au film, single layer AuNPs and Au NPs/graphene/AuNPs. (b) Corresponding electrical field energy distribution of the Au NPs/graphene/AuNPs hybrid structure. The diameters of the first layer Au NPs are 40 nm and the second layer Au NPs are 60 nm, respectively. (c) Reflectance as a function of Au NPs diameter in the second layer. (d) Magnified electrical field energy distribution of Au NPs/graphene/AuNPs hybrid structure with different diameters of Au NPs in the second layer.

Besides morphology, we also simulated the effect of different horizontal distances between the adjacent Au NPs on the reflectance and electric field distribution. The FDTD simulation results disclose that with the increase of distance, the reflectance will be decreased accordingly (Fig. 6a). In other words, Au NPs /graphene/Au NPs with relatively large distance can suppress reflectance and confine incident light, which is highly beneficial for conversion efficiency (Fig. 6 (b-f)).

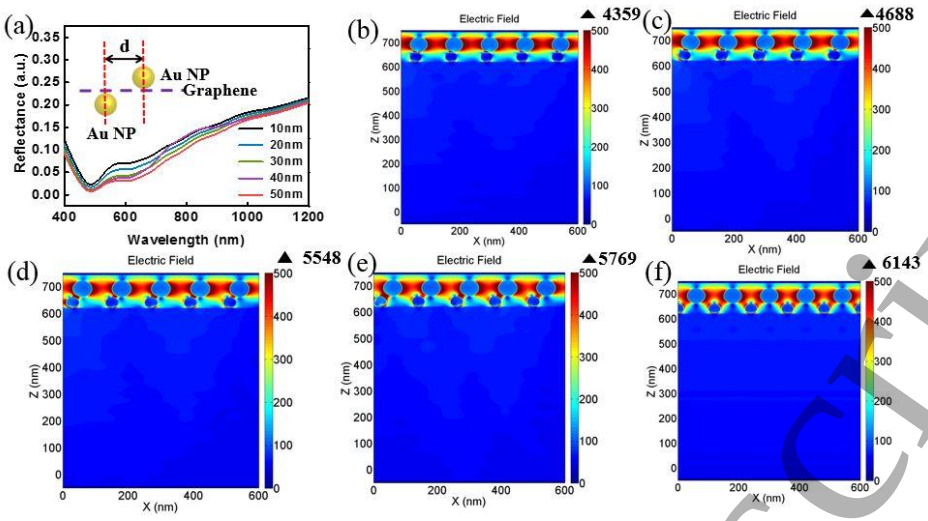

Figure 6 (a) Simulated reflectance of Au NPs/graphene/AuNPs hybrid structure with different horizontal distance of the AuNPs in the first layer and second layer. (b-f) Electrical field energy distribution of Au NPs/graphene/AuNPs hybrid structure with different horizontal distance of the AuNPs in the first layer and second layer. The distance is 10nm (b), 20nm(c), 30nm(d), 40nm(e), and 50nm (f) respectively.

As discussed above, it is revealed that the distinct structure of the Au NPs/graphene/Au NPs electrode exhibits strong light confinement effect, which is helpful for the conversion of photons to electricity. As a matter of fact, the dual-plasmon enhanced Si Schottky photodetector D3 also exhibits strong dependence dependence on the intensity of excitation light of different wavelength, including 365nm (Fig. S3), 532nm (Fig. 7), 980nm (Fig. S4), and 1330nm (Fig. S5). Figure 7a plots the time-resolved photoresponse of D3 under a light source of 532nm wavelength with intensity varying from 0 to 8.6μW/cm^2 at 0 V bias. When the light intensity is 790 nW/cm^2, its on/off ratio is about 10^2, showing considerable response to this low intensity. However, according to power law $I_{photo} = AP^{\theta}$[41], fitting of the current density shows sublinearity to the light power (Fig. 7b). This is probably because the light absorption of Au NPs and graphene will lead to temperature rise with the increase of light strength, which will promote the recombination of electrons and holes[19].

The corresponding respectivty (R), detectivity (D*) and external quantum efficiency (EQE)

of the device were further computed based on the dependence of photocurrent over light intensity (Fig. 7(c-d)). Specific detectivity $D^*(=RS^{1/2}/(2qI_{dark})^{1/2})$ describes the smallest detectable signal of the photodetector[9]. And the external quantum efficiency EQE(=hcRλ/(qλ)) presents the number of electrons probed per incident photon[42]. It is showed that the R and D* both decrease with the light intensity and reach saturation, which is consistent with previous report [19]. At weak light intensity, a large number of hot electrons will generate under illumination, while thermal effect is still small, leading to higher R and D*. When the light intensity increases, thermal effect becomes strong causing the saturation of photoresponse. The D* and EQE can reach about 2.4×10^{13} Jone and 20% under the illumination of 532 nm at the lowest incident power, respectively.

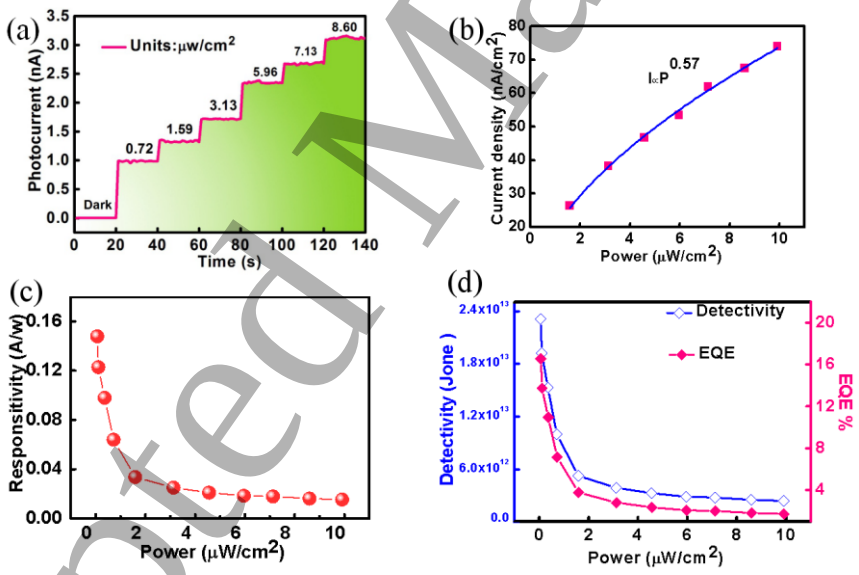

Figure 7 (a) Time-resolved photoresponse of D3 under different excitation intensity at wavelength of 532 nm. The bias voltage was fixed at 0V. (b) The photocurrent of the device relative to the light intensity density at zero bias voltage.(c-d) Plots of responsivity, detectivity and EQE of D3 as a function of light intensity.

Another important metric for photodetector is the transient photoresponse, which was characterized using a chopper-generated short light pulse (Fig. 8a). Figure 8b shows the

normalized transient photocurrent of D1, D2 and D3 measured under a pulsed frequency of 10 kHz at bias of 0V. Compared with D1 and D2, the transient response of D3 are flat with sharper rise and fall edges. The relatively fast respond speed of D3 should be the result of its high strength hot spot, which can produce electrons of larger energy with higher speed[16]. A set of photocurrents in D3 versus time scans at different frequency were shown in Figure 8c. The response exhibits long-term repeatability in the frequency range from 10 kHz to 1MHz. A single normalized cycle of 1MHz shows a rise time of 360ns and a relatively faster decay time of 330ns (Fig. 8d). The shorter decay time means there should be less trap or defect states involved in the process for the high crystal quality of c-Si and graphene[2]. And there are a fast component of 244 ns and a slow component of 86 ns in the decay process of photocurrent. This maybe be caused by the existence of two factors (thermalization or recombination with hole) for the annihilation of electron[16][43], in consistence with previous analysis of energy band diagram. The corresponding 3dB bandwidth (B) of D3 is obtained to be 780kHz, which is far above the value required for imaging applications[44] (Fig. 8e). And with the frequency increasing, the noise current (i_n) decreases and reaches about 1 $pA \cdot Hz^{-1/2}$. Based on it, the noise equivalent power ($NEP=i_n \times B^{1/2}/R$) is calculated to be 1.6×10^{-8} W at zero bias (780kHz), which represents the minimum optical input power that the device can distinguish from the noise[45]. Table 1 summarizes some key parameters of the present dual-plasmon enhanced Schottky photodetector and other devices. It can be easily found that even though the detectivity of our device is lower than the majority of the devices listed in Table 1, the detetecivity is however highly competitive. In addition, the response time is faster than most of devices composed of ZnONW/array Si, plasmon-enhanced

graphene/GaAs, SQ NW/c-Si, and SWCNTs/PC71BM.

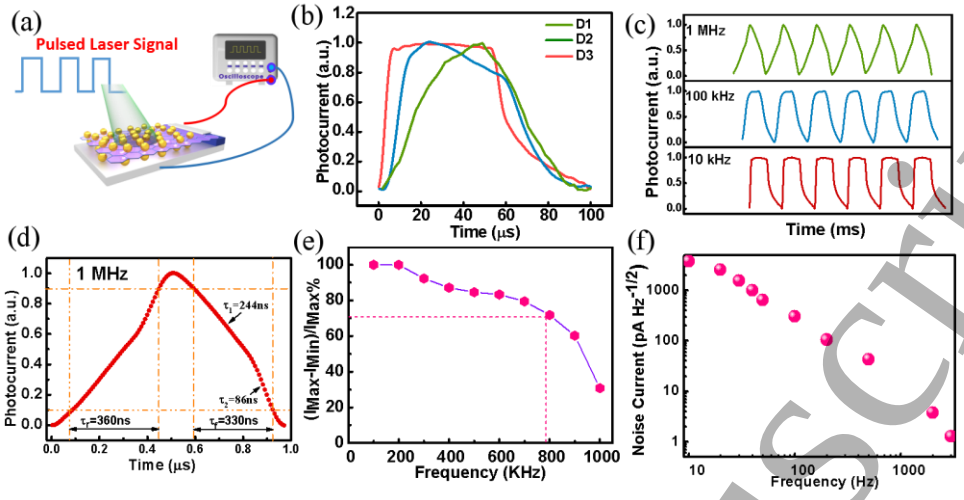

Figure 8 (a) Schematic illustration of the measurement configuration for the photoresponse speed detection. (b)Normalized photoresponse characteristic of D1,D2 and D3 at a pulsed frequency of 10 kHz at wavelength of 532 nm. (c) Response of D3 to pulsed light irradiation at frequencies of 10 kHz, 100 kHz and 1 MHz at wavelength of 532 nm. (d) Enlarged photoresponse peak for estimating the rise time (τ_r) and fall time (τ_f).(e) Relative balance $(I_{max}/I_{min})/I_{max}$ versus switching frequency. (f) The dark noise current of the D3 measured at different frequencies at zero bias.

Table 1. Comparison of the key parameters of the dual-plasmon enhanced Si Schottky photodetector and other devices.

Photodetector	Light (nm)	R[mA/W]	D*@V_{bia} [$\times10^{11}$Jones]	Rise time and Decay time	Reference
Dual plasmon photodetector	365-1330	24.17-109.69	2.4-16@0V	360ns,330ns	This work
SWCNTs/PC71BM	400−1010	20-260	0.2−2@0 V	0.3s	[46]
Plasmon-enhanced graphene/GaAs	325−980	210	298@6V	1 s	[47]
Pt NPs modified graphene/Si	400−900	~26000		78ns	[48]
ZnO NW arrays/p-Si	442 − 1060	200-800	@-2V	0.84 ms,1.28 ms	[7]
SQ NW/c-Si	254−980	1300−9800	0.06−0.45@−3 V	0.6s,0.4s	[2]

4. Conclusion

In summary, we have proposed and experimentally demonstrated a dual-plasmon

enhanced Si Schotty photodetector by using a hybrid Au NPs/graphene/Au NPs electrode, which can effectively enhance localized electric field in the resonant and off-resonant wavelength region and improve the light trapping ability of device. It is worth mentioning that such a structure is beneficial for the tunneling of hot electrons, contributing to a larger photocurrent. Without texturing the surface of planar Si, the detecting wavelength region of detector were broadened to be from UV to near-infrared light (360-1330nm) with improved responsivity. Further analysis found that the dual-plasmon enhanced photodetector exhibits high response speed and good performance at high frequency optical signal. Its simple and large-area preparation processes make the photodetector suitable for large-scale versatile multi-wavelength imager and safety monitoring applications.

Acknowledgments

This work is received financial support from the National Natural Science Foundation of China (61675062, 61575059), National Key Research and Development Program of China (2016YFC0102401), Anhui Provincial Natural Science Foundation (1708085MA24), Fundamental Research Funds for the Central Universities of China (2015HGZX0027), and the Fundamental Research Funds for Graphene (W2016JSKF0207).

References

[1] Qianqian L, Ardalan A, Paul L B and Paul M 2015 Filterless narrowband visible photodetectors *Nature Photonics* **9** 687 – 94

[2] Wei D, Jiansheng J, Qixun S, Jincheng W, Xiujuan Z, Shenwen Y, Qing Z and Xiaohong Z 2015 Organic Nanowire/Crystalline Silicon p–n Heterojunctions for High-Sensitivity, Broadband Photodetectors *ACS Appl. Mater. Interfaces* **7** (3) 2039 – 45

[3] Konstantatos G and Sargent E H 2010 Nanostructured materials for photon detection *Nat. Nanotechnol.* **5** 391-400

[4] Monroy E, Omnès F and Calle F 2003 Wide-bandgap semiconductor ultraviolet photodetectors Semicond. *Sci. Tech.* **18** R33

[5] Canjeevaram Balasubramanyam R K, Kandjani A E, Harrison C J, Abdul Haroon Rashid S S A, Sabri Y M, Bhargava S K, Narayan R, Basak P and Ippolito S J 2017 1,4-Dihydropyrrolo[3,2-b]pyrroles as a Single Component Photoactive Layer: A New Paradigm for Broadband Detection *ACS Appl. Mater. Interfaces* **9** 27875-82

[6] Gu L and Fan Z 2017 Perovskite/organic-semiconductor heterojunctions for ultrasensitive photodetection Light *Sci. Appl.* **6** e17090

[7] Zou H, Li X, Peng W, Wu W, Yu R, Wu C, Ding W, Hu F, Liu R, Zi Y, Wang ZL 2017 Piezo-Phototronic Effect on Selective Electron or Hole Transport through Depletion Region of Vis-NIR Broadband Photodiode *Advanced Materials* 1701412

[8] Qi Z, Zhai Y, Wen L, Wang Q, Chen Q, Iqbal S, Chen G, Xu J and Tu Y 2017 Au nanoparticle-decorated silicon pyramids for plasmon-enhanced hot electron near-infrared photodetection *Nanotechnology* **28** 275202

[9] Wan X, Xu Y, Guo H, Shehzad K, Ali A, Liu Y, Yang J, Dai D, Lin C-T, Liu L, Cheng H-C, Wang F, Wang X, Lu H, Hu W, Pi X, Dan Y, Luo J, Hasan T, Duan X, Li X, Xu J, Yang D, Ren T and Yu B 2017 A self-powered high-performance graphene/silicon ultraviolet photodetector with ultra-shallow junction: breaking the limit of silicon? *npj 2D Mater. Appli.* **1** 4

[10] Li X M, Bi M H, Cui L, Zhou Y Z, Du X W, Qiao SZ an d Yang J 2017 3D Aluminum Hybrid Plasmonic Nanostructures with Large Areas of Dense Hot Spots and Long-Term Stability *Adv. Funct. Mater.* **27** 1605703

[11] Eshwar T, Ashok K S, Sanjay K S and Vamsi K K 2014 Internal quantum efficiency analysis of plasmonic textured silicon solar cells: surface plasmon resonance and off-resonance effects *J. Phys. D Appl. Phys. 47* 425101

[12] Brongersma M L, Halas N J and Nordlander P 2015 Plasmon induced hot carrier science and technology *Nat.Nanotechnol.* **10** 25–34

[13] Li W and Valentine J G 2017 Harvesting the loss: surface plasmon-based hot electron photodetection *Nanophotonics* **6** 177–91

[14] Luo L B, Huang X L, Wang M Z, Xie C, Wu C Y, Hu J G, Wang L and Huang J A 2014 The effect of plasmonic nanoparticles on the optoelectronic characteristics of CdTe nanowires *Small* **10** 2645-52

[15] Elżbieta R, Michał K and Henryk D 2016 Nanostructured zinc oxide systems with gold nanoparticle pattern for efficient light trapping *J. Phys. D Appl. Phys.* **49** 045104

[16] Harutyunyan H, Martinson A B, Rosenmann D, Khorashad L K, Besteiro L V, Govorov A O and Wiederrecht G P 2015 Anomalous ultrafast dynamics of hot plasmonic electrons in nanostructures with hot spots *Nat. Nanotechnol.* **10** 770-4

[17] Zhao Y, Li X, Du Y, Chen G, Qu Y, Jiang J and Zhu Y 2014 Strong light-matter interactions in sub-nanometer gaps defined by monolayer graphene: toward highly sensitive SERS substrates *Nanoscale* **6** 11112-20

[18] Zhi Q W, Jing L Y, Nallappagar K. M, Yue J Z, Si R F, Yang H L, Jiang H W, Wei W Z, Cai Y Q, Jian F L, Shi S L 2018 Gap-Mode Surface-Plasmon-Enhanced Photoluminescence and Photoresponse of MoS2 *Advanced Materials* **30** 1706527

[19] Du B, Lin L, Liu W, Zu S, Yu Y, Li Z, Kang Y, Peng H, Zhu X and Fang Z 2017 Plasmonic hot electron tunneling photodetection in vertical Au-graphene hybrid nanostructures *Laser Photonics Rev.* **11** 1600148

[20] Eda G and Chhowalla M 2011 Graphene patchwork *ACS Nano.* **5** 4265-8

[21] Xin M L, Hong W Z 2016 The graphene-semiconductor Schottky junction *Physics Today* **69** 46-51

[22] Li X M, Zhu M, Du M D, Lv Z, Zhang L L, Yuan C Y, Yao Y, Ting T L, Li X, Wang K L, Zhu H W, Fang Y 2016 High Detectivity Graphene-Silicon Heterojunction Photodetector *Small* **12** 595-601

[23] Chen Z.F., Li X.M., Wang J.Q., Tao L. , Long M.Z., Liang S.J., Lay K. A., Shu C., Tsang H.K., Xu J.B. 2017 Synergistic effects of plasmonics and electron trapping in graphene short-wave infrared photodetectors with ultrahigh responsivity. *ACS Nano* **11** 430−437

[24] Echtermeyer T.J., Britnell L., Ferrari A.C. , Jasnos P.K., Novoselov K.S.,Lombardo A.,Gorbachev R.V., Grigorenko A.N., Geim A.K. 2011 Strong plasmonic enhancement of photovoltage in graphene. *Nature Communications* **2** ncomms1464

[25] Xu G.W. , Liu J.W., WangQ., Hui R.Q.,Chen Z.J., Maroni V. A., Wu J. 2012 Plasmonic Graphene Transparent Conductors. *Advanced Materials* **24** OP71-OP76

[26] Xu G.W., Lu R.,Liu J.W. , Chiu H.Y. ,Hui R.Q. , and Wu J.Z. 2014 Photodetection Based on Ionic Liquid Gated Plasmonic Ag Nanoparticle/Graphene Nanohybrid Field Effect Transistors. *Adv. Optical Mater.* **2** 729 – 736

[27] Robak E, Grześkiewicz B and Kotkowiak M 2014 Absorption enhancement in silicon nanowire-optical nanoantenna system for photovoltaic applications *Opt. Mater.* **37** 104-9

[28] Casiraghi C 2011 Raman intensity of graphene *phys. status solidi B* **248** 2593-7

[29] Nie B, Hu J G, Luo L B, Xie C, Zeng L H, Lv P, Li F Z, Jie J S, Feng M, Wu C Y, Yu Y Q and Yu S H 2013 Monolayer graphene film on ZnO nanorod array for high-performance Schottky junction ultraviolet photodetectors *Small* **9** 2872-9

[30] Goykhman I, Sassi U, Desiatov B, Mazurski N, Milana S, de Fazio D, Eiden A, Khurgin J, Shappir J, Levy U and Ferrari A C 2016 On-Chip Integrated, Silicon-Graphene Plasmonic Schottky Photodetector with High Responsivity and Avalanche Photogain *Nano. Lett.* **16** 3005-13

[31] Liao L, Peng H and Liu Z 2014 Chemistry makes graphene beyond graphene *J. Am. Chem. Soc.* **136** 12194-200

[32] Lu R., Konzelmann A., Xu F., Gong Y.P., Liu J.W.,Liu Q.F.,Xin M.,Hui R.Q., Wu J. Z. 2015 High sensitivity surface enhanced Raman spectroscopy of R6G on in situ fabricated Au nanoparticle/graphene plasmonic substrates *Carbon* **86** 78-85

[33] Omori E, Shimizu H and Ikeda M 2007 Analysis of Au/Si Schottky barrier type AC surface photovoltage in silicon wafer surface dipped into Au aqueous solution Electron *Comm. JPN* **2** 90 27-33

[34] Irmscher K, Galazka Z, Pietsch M, Uecker R and Fornari R 2011 Electrical properties of β-Ga2O3 single crystals grown by the Czochralski method *J. Appl. Phys.* **110** 063720

[35] Fathy N, Ichimura M 2005 Photoelectrical properties of ZnS thin films deposited from aqueous solution using pulsed electrochemical deposition. *Sol Energy Mater Sol* **87** 747–56.

[36] Manna S, Das S, Mondal S P, Singha R and Ray S K 2012 High efficiency Si/CdS radial nanowire heterojunction photodetectors using etched Si nanowire templates *J. Phys.Chem. C* **116** 7126–33

[37] Zeng L, Xie C, Tao L, Long H, Tang C, Tsang Y H and Jie J 2015 Bilayer graphene based surface passivation enhanced nano structured self-powered near-infrared photodetector *Opt. Express* **23** 4839–46

[38] Lim D K, Jeon K S, Kim H M, Nam J M and Suh Y D 2010 Nanogap-engineerable Raman-active nanodumbbells for single-molecule detection *Nat. Mater.* **9** 60-67

[39] Osberg K D, Rycenga M, Harris N, Schmucker A L, Langille M R, Schatz G C and Mirkin C A 2012 Dispersible gold nanorod dimers with sub-5 nm gaps as local amplifiers for surface-enhanced Raman scattering *Nano. Lett.* **12** 3828-32

[40] Zhu X, Shi L, Schmidt M S, Boisen A, Hansen O, Zi J, Xiao S and Mortensen N A 2013 Enhanced light-matter interactions in graphene-covered gold nanovoid arrays *Nano. Lett.* **13** 4690-6

[41] Joshi N 1990 Photoconductivity: *art: science & technology* vol 25: CRC Press

[42] Kong W Y, Wu G A, Wang K Y, Zhang T F, Zou Y F, Wang D D and Luo L B 2016 Graphene-beta-Ga2 O3 Heterojunction for Highly Sensitive Deep UV Photodetector Application *Adv. Mater.* **28** 10725-31

[43] Guo F, Yang B, Yuan Y, Xiao Z, Dong Q, Bi Y and Huang J 2012 A nanocomposite ultraviolet photodetector based on interfacial trap-controlled charge injection *Nat. Nanotechnol.* **7** 798-802

[44] Lin Q, Armin A, Burn P L and Meredith P 2015 Filterless narrowband visible photodetectors *Nat. Photonics* **9** 687-94

[45] Armin A, Hambsch M, Kim I K, Burn P L, Meredith P and Namdas E B 2014 Thick junction broadband organic photodiodes *Laser Photonics Rev.* **8** 924-32

[46] Xie Y., Gong M. G.,Shastry T. A., Lohrman J., Hersam M.C., Ren S. Q. 2013 Broad-Spectral-Response Nanocarbon

Bulk-Hetero-junction Excitonic Photodetectors. *Adv. Mater.* **25** 3433−3437

[47] Lu Y.H., Feng S., Wu Z.Q., Gao Y.X., Yang J.L., Zhang Y.J., Hao Z.Z., Li J.F., Li E., Chen H.S., Lin S.S. 2018 Broadband surface plasmon resonance enhanced self-powered graphene/GaAs photodetector with ultrahigh detectivity. *Nano Energy* **47** 140-149

[48] Huang K., Yan Y.C., Li K., Khan A., Zhang H., Pi X.D., Yu X.G., Yang D., 2018 High and Fast Response of a Graphene-Silicon Photodetector Coupled with 2D Fractal Platinum Nanoparticles *Adv. Optical Mater.* **6** 1700793